11th World Congress on Computational Mechanics (WCCM XI)
5th European Conference on Computational Mechanics (ECCM V)
6th European Conference on Computational Fluid Dynamics (ECFD VI)
E. Oñate, J. Oliver and A. Huerta (Eds)

A TWO-FLUID COMPUTATIONAL MODEL TO STUDY MAGNETIC RECONNECTION IN REACTIVE PLASMAS UNDER CHROMOSPHERIC CONDITIONS

A. Alvarez Laguna[1*], A. Lani[1], N. N. Mansour[2], A. Kosovichev[3], S. Poedts[4]

[1] Von Karman Institute for Fluid Dynamics, Waterloosesteenweg 72, 1640 Sint Genesius Rode, Belgium, alejandro.alvarez.laguna@vki.ac.be, lani@vki.ac.be
[2] NASA Ames Research Center, MS 230-3, Moffett Field, CA 94035, USA, Nagi.N.Mansour@nasa.gov
[3] Big Bear Solar Observatory, 40386 North Shore Lane, Big Bear City, CA 92314-9672, USA sasha@bbso.njit.edu
[4] Centre for mathematical Plasma-Astrophysics, KU Leuven, Celestijnenlaan 200b, 3001 Heverlee, Belgium, Stefaan.Poedts@wis.kuleuven.be

Key words: Plasma, Solar Physics, Finite Volume Method, Magnetohydrodynamics (MHD), Multi-fluid, Magnetic reconnection

Abstract. We use a two-fluid (plasma + neutrals) model to simulate the magnetic reconnection in chromospheric conditions. Improved models for characterizing collisional and reactive magnetized partially ionized plasma in the presence of electromagnetic fields are essential to understand the phenomena taking place in astrophysical and laboratory plasmas. Particularly, scenarios where dissipative processes and thermo-chemical non-equilibrium play an important role are beyond the classical single-fluid MHD representation. The governing equations of the multi-fluid model used include two loosely-coupled systems: the reactive two-fluid equations and the full Maxwell equations complemented with two additional divergence cleaning equations for enforcing numerically the two Gauss's laws. A second-order cell-centered Finite Volume method for unstructured grids is used to discretize both systems. In particular, a variant of the AUSM$^+$-up scheme is used to tackle the two-fluid equations, while Steger-Warming scheme is chosen for treating Maxwell equations. The unsteady simulation is advanced in time with an implicit three-point Backward Euler scheme. Results of the reconnection process are presented showing clear differences in the velocities and path of the neutrals compared to the ions that respond to the effect of the electromagnetic fields. Also shown are the different evolutions of the density of neutrals and ions that interact through chemical reactions.

1 INTRODUCTION

The study of plasma in the presence of electromagnetic fields offers potential developments in areas like astrophysics, laboratory plasmas, hypersonic reentry vehicle design or propulsion. The governing equations describing ionized flows in presence of strong electromagnetic fields are Navier-Stokes coupled with Maxwell equations. This set leads to a stiff system, difficult to solve since it comprises characteristic speeds spanning from the speed of light to the speed of sound. Including the time dependent term of Maxwells equations allows considering as well the high frequency changes of the electromagnetic field induced by the movement of the conducting flow. Usually, the single-fluid MHD models assume this changes to be negligible, adding thus some degree of uncertainty [9].

Another limitation of the standard single-fluid MHD models is observed when studying scenarios of finite conductivity where dissipative effects are important. Particularly, magnetic reconnection is a diffusion driven process in which those models have shown strong disagreement with experimental and observational data. However, it is a phenomenon of significant interest since it has since long been considered as a mechanism for creating transient phenomena in magnetized plasma. It occurs when oppositely directed magnetic field lines in conducting plasma merge due to diffusive processes producing a change of topology. The rearrangement of magnetic field lines produces a change of the magnetic flux that creates a current sheet due to the finite conductivity. In addition, the reconnection process causes a conversion of magnetic energy into kinetic and thermal energy, heating up the flow and accelerating it to very high speed in very small timescales.

There are a wide variety of astrophysical scenarios in which the magnetic reconnection plays an important role. It is considered to be a likely mechanism that heats the corona to a few million degrees, still one of the biggest unsolved mysteries in heliophysics [10]. Also, in coronal mass ejections (CMEs) and solar flares it is considered as a triggering mechanism which is present during the onset and early stages of the ejection [11]. In the Earths magnetosphere it is said to produce the plasma outflow at the magnetotail that is driven by the Earths magnetic field into the atmosphere producing the aurora borealis and geomagnetically induced currents (GICs) [12].

In the present work, we will focus on studying the magnetic reconnection in the Sun chromosphere, following the work presented in [1]. Observational data [8] have unveiled that the magnetic reconnection is the driver mechanism for chromospheric jets and the spicules. The former can have timescales of 200-1000 s and current sheet length scales up to 5 Mm, producing outflows of 10 km/s. On the other hand, the spicules are smaller but faster phenomena, that last 10-600 s in length scales up to 1 Mm causing outflows up to 20-150 km/s [1].

The present ongoing research is targeted towards the development of consistent and effective models of magnetic reconnection by considering multi-fluid models and accounting for the influence of the electromagnetic fields. The improvement of the magnetic reconnection modeling would have a direct impact on our ability to model CMEs.

2 MODELING OF THE MAGNETIC RECONNECTION

Magnetic reconnection is a process that happens as a result of a diffusive mechanism that produces a decay in the electrical conductivity of the plasma. The frozen-in constrain that holds in ideal plasmas (with infinite conductivity) is broken in a small region of width δ and length L. In this region, the magnetic field lines reconnect producing a rate of magnetic flux that results in the formation of a current sheet. Thus, the non-dimensional magnetic reconnection rate is defined [13] as follows:

$$M = \frac{d\Phi/dt}{v_A B_i} \tag{1}$$

where Φ is the magnetic flux per unit length in the direction perpendicular to the plane containing the current sheet , v_A is the Alfven speed and B_i is the magnetic field evaluated upstream of the current sheet.

Therefore, classical ideal MHD equations assuming the conductivity to be infinite are not able to tackle the physics involved in the reconnection. Nevertheless, the resistive singlefluid theory has developed analytical models for 2D steady magnetic reconnection. The Sweet-Parker model [14] proposes a non-dimensional reconnection rate of the form:

$$M = R_m^{-1/2} \tag{2}$$

where

$$R_m = v_A L/\eta \tag{3}$$

is called the Lundquist number, and η is the resistivity.

However, the model is unable to explain the fast energy released by the solar flares or in chromospheric jets and spicules, providing reconnection rates several orders of magnitude smaller.

On the other hand, the Petschek model [15] predicts faster reconnections suggesting geometry different from the Sweet-Parker one, Eq. 4. However, the model assumes explicitly or tacitly that resistivity gives the configuration setup. Because of this controversial issue, the Petschek model has been gradually rejected [16].

$$M = \frac{\pi}{8\ln(R_m)} \tag{4}$$

Therefore, it is necessary to consider alternative theories to model the reconnection. Multi-fluid models consider each particle species as a different fluid that interact with each other by means of collisions and chemical reactions, exchanging thus mass, momentum and energy in their interplay. Therefore, since the width of the diffusion region can be comparable to the ion scales [12], the multi-fluid description are considered to capture diffusive effects that are completely neglected by the single-fluid theory.

In the literature, one can find several fluid closures accounting for the different behavior of the species of plasmas in presence of electromagnetic fields. Braginskii [17] derives a two-fluid formulation considering separate ions and electrons. In his seminal work, he proposes closures for the transport properties, accounting for the anisotropy introduced by the magnetic field. Similarly, Magin [18] proposes a multi-component model separating heavy particles and electrons, treating the effect of the magnetic field on the transport properties. Most recently, Meier [2] has proposed a two-fluid model considering the charged particles and neutrals as separate fluids, considering both anisotropic effects in the plasma heat conduction due to the magnetic field and chemical reactions (ionization and recombination).

3 GOVERNING EQUATIONS

The multi-fluid description used in the results shown hereafter is the model discussed in [2]. The latter is a two-fluid model that considers separately neutrals and charged species, i.e. hydrogen ions and electrons. The full set of equations considered comprises mass, momentum and total energy conservation for both fluids. The chemical reactions considered are electron impact ionization and radiative recombination. The excited states are not tracked, only an effective potential is assumed ϕ_{ion} for the ionization reaction. The plasma is assumed to be optically thin, so the radiation effects are completely lost from the system. Electrons are considered to be in thermal equilibrium with ions, allowing neutrals to be in non-LTE. Charge neutrality is assumed and the electrons inertia and viscosity is neglected. This simplifications yields the following system:

$$\frac{\partial \rho_i}{\partial t} + \nabla \cdot (\rho_i \vec{v}_i) = m_i(\Gamma_i^{ion} + \Gamma_i^{rec}), \tag{5}$$

$$\frac{\partial \rho_n}{\partial t} + \nabla \cdot (\rho_n \vec{v}_n) = m_n(\Gamma_n^{ion} + \Gamma_n^{rec}), \tag{6}$$

$$\frac{\partial \rho_i \vec{v}_i}{\partial t} + \nabla \cdot (\rho_i \vec{v}_i \vec{v}_i + p_i \vec{\vec{\delta}} + p_e \vec{\vec{\delta}}) = -\nabla \cdot (\pi_i) + \vec{j} \times \vec{B} + \vec{R}_i^{in} + \Gamma_i^{ion} m_i \vec{v}_n - \Gamma_n^{rec} m_i \vec{v}_i, \tag{7}$$

$$\frac{\partial \rho_n \vec{v}_n}{\partial t} + \nabla \cdot (\rho_n \vec{v}_n \vec{v}_n + p_n \vec{\vec{\delta}}) = -\nabla \cdot (\pi_n) - \vec{R}_i^{in} - \Gamma_i^{ion} m_i \vec{v}_n + \Gamma_n^{rec} m_i \vec{v}_i, \tag{8}$$

$$\begin{aligned} \frac{\partial}{\partial t}\left(\varepsilon_i + \frac{p_e}{\gamma_e - 1}\right) + \nabla \cdot \left(\varepsilon_i \vec{v}_i + \frac{\gamma_e p_e}{\gamma_e - 1}\vec{v}_i + p_i \vec{v}_i\right) = -\nabla \cdot (\vec{v}_i \cdot \pi_i + \vec{q}_i + \vec{q}_e) + \vec{j} \cdot \vec{E} + \vec{v}_i \vec{R}_i^{in} \\ + Q_i^{in} - \Gamma_n^{rec} \frac{1}{2} m_i v_i^2 - Q_n^{rec} + \Gamma_i^{ion}\left(\frac{1}{2} m_i v_n^2 - \phi_{ion}\right) + Q_i^{ion}, \end{aligned} \tag{9}$$

$$\frac{\partial \varepsilon_n}{\partial t} + \nabla \cdot (\varepsilon_n \vec{v}_n + \vec{v}_n p_n) = -\nabla \cdot (\vec{v}_n \cdot \pi_n + \vec{q}_n) - \vec{v}_n \vec{R}_i^{in} + Q_n^{in} + \Gamma_n^{rec} \frac{1}{2} m_i v_i^2 + Q_n^{rec} - \Gamma_i^{ion} \frac{1}{2} m_i v_n^2 - Q_i^{ion} \quad (10)$$

Where the subindices i, e, n stand for ions, electrons and neutrals. The electrical current follows Ohm's law $\vec{E} + \vec{v}_i \times \vec{B} = \eta \vec{j}$ with the resistivity η assumed to be constant. The reaction rates Γ^{ion} and Γ^{rec} and the reaction energy production Q^{ion} and Q^{rec} are taken from [24] and [25]. The momentum and energy collisional terms $\vec{R}_\alpha^{\alpha\beta}$ and $Q_\alpha^{\alpha\beta}$ considered are discussed in [1]. Ions and neutrals viscosity stress tensor are assumed to be Newtonian, with constant viscosity. Neutrals heat conduction follows Fouriers law with constant thermal conductivity, whereas ions have anisotropic heat flux accounting for the effect of the magnetic field, described in [17]. The fluid are assumed to be perfect gases with a constant $\gamma = 5/3$.

The electromagnetic influence is tackled with the Maxwell equations:

$$\frac{\partial \vec{B}}{\partial t} + \nabla \times \vec{E} = 0 \quad (11)$$

$$\frac{\partial \vec{E}}{\partial t} - c^2 \nabla \times \vec{B} = -\frac{\vec{j}}{\epsilon_0} \quad (12)$$

$$\nabla \cdot \vec{B} = 0 \quad (13)$$

$$\nabla \cdot \vec{E} = \frac{\rho_c}{\epsilon_0} \quad (14)$$

where ρ_c is the charge density that is assumed to be zero.

4 NUMERICAL MODELING

4.1 Finite Volume Method

Our numerical results have been obtained using the Finite Volume (FV) solver for unstructured grids provided by the COOLFluiD platform [5, 6, 19, 7]. The governing equations are written in conservative form, as follows:

$$\frac{d}{dt} \int_{\Omega_i} \mathbf{U} \, d\Omega + \oint_{\partial\Omega_i} \mathbf{F^c} \cdot \mathbf{n} \, d\Sigma = \oint_{\partial\Omega_i} \mathbf{F^d} \cdot \mathbf{n} \, d\Sigma + \int_{\Omega_i} \mathbf{S} \, d\Omega \quad (15)$$

The conservative form of Maxwell equations is found in [9]. The cell-centered FV discretization applies the integral conservation law to each cell, assuming the solution to be constant over the cell and storing the value at the centroid of the cell. In order to obtain

second-order accuracy in space, inverse-distance weighted least square reconstruction [20] is used. The multidimensional limiter of Venkatakhrisnan [21] is used to obtain oscillation free solutions. The discretization of the inviscid fluxes is explained section 4.3.

4.2 Hyperbolic divergence cleaning for Maxwell equations

One of the biggest concerns in the development of a Maxwell solver is to satisfy the two divergence constrains Eq. 13 and Eq. 14 on the discrete level. The hyperbolic divergence cleaning method [3] is a proven efficient way to enforce the constrains in Finite Volume solvers. Two lagrange multipliers ϕ and ψ are added in Maxwell equations as follows:

$$\frac{\partial \vec{B}}{\partial t} + \nabla \times \vec{E} + \gamma^2 \nabla \Psi = 0 \tag{16}$$

$$\frac{\partial \vec{E}}{\partial t} - c^2 \nabla \times \vec{B} + \chi^2 c^2 \nabla \Phi = -\frac{\vec{j}}{\epsilon_0} \tag{17}$$

$$\frac{\partial \Psi}{\partial t} + c^2 \nabla \cdot \vec{B} = 0 \tag{18}$$

$$\frac{\partial \Phi}{\partial t} + \nabla \cdot \vec{E} = \frac{\rho_c}{\epsilon_0} \tag{19}$$

Artificial waves are introduced at speeds γc and χc that remove the errors in the fulfillment of the constrains.

4.3 Steger-Warming scheme for Maxwell equations

The Steger-Warming scheme [22] splits the flux at the interface into positive and negative components based on the eigenvalue structure of the system as follows:

$$\mathbf{F^c} = \mathbf{A}_+ \mathbf{U}^L + \mathbf{A}_- \mathbf{U}^R \tag{20}$$

where

$$\mathbf{A} = \frac{\partial \mathbf{F^c}}{\partial \mathbf{U}} = \mathbf{A}_- + \mathbf{A}_+ \text{ and } \mathbf{A}_\pm = \mathbf{R} \Lambda_\pm \mathbf{R}^{-1} \tag{21}$$

$\mathbf{R}$ is the matrix of right eigenvectors, $\Lambda_\pm$ the diagonal matrix of diagonal matrices with the positive and negative eigenvalues, $\mathbf{U}$ are the conservative variables. In the hyperbolic divergence cleaning Maxwell system $\mathbf{U} = (B_x, B_y, B_z, E_x, E_y, E_z, \Psi, \Phi)$ and the eigenvalues are $\lambda = c, c, -c, -c, \chi c, -\chi c, \gamma c, -\gamma c$. The details of the discretization including the divergence cleaning method are discussed in [3]. The method is shown to work standalone and coupled with Navier-Stokes equations of a single conducting fluid [23].

4.4 AUSM scheme for fluid equations

In the results shown hereafter, the inviscid flux of the multi-fluid Navier-Stokes is discretized using the AUSM$^+$-up scheme. This method, discussed in [4] is originally designed for single-fluid and in this work it is adapted for multi-fluid. The scheme splits the inviscid flux of each fluid at the cell interface into the convective part and the pressure flux as follows:

$$\mathbf{F_s^c} = \mathbf{F_s^{conv}} + \mathbf{P_s} = \dot{m}_s \mathbf{\Psi_s} + \mathbf{P_s} \tag{22}$$

The subindex $s = i, n$ denotes the fluid considered, i.e. ions or neutrals for the model discussed in the previous section. $\dot{m}_s$ is the mass flux of the species s, $\mathbf{\Psi_s}$ is a vector with the convected variables and $\mathbf{P_s}$ is the pressure flux. The latter can be expressed as:

$$\dot{m}_s = \rho_s q_s, \quad \mathbf{\Psi} = (1,\ \mathbf{u},\ h)_s, \quad \mathbf{P_s} = (0, p_s \mathbf{n}, 0) \tag{23}$$

where $q_s = \mathbf{u} \cdot \mathbf{n}$ is the velocity of the fluid s projected onto the normal $\mathbf{n}$ of the considered cell interface.

The numerical discretization of the flux $\mathbf{F_s^c}$ at the interface between the left (L) and right (R) states is defined as:

$$\mathbf{F^c_{s_{1/2}}} = \dot{m}_{s_{1/2}} \mathbf{\Psi_s^{L/R}} + \mathbf{P_{s_{1/2}}} \tag{24}$$

Simple upwinding is applied to define $\mathbf{\Psi_s^{L/R}}$:

$$\mathbf{\Psi} = \begin{cases} (1,\ \mathbf{u},\ h)_s^L & \text{if } \dot{m}_{s_{1/2}} > 0 \\ (1,\ \mathbf{u},\ h)_s^R & \text{otherwise} \end{cases} \tag{25}$$

The methods to compute the numerical mass flux $\dot{m}_{s_{1/2}}$ and the pressure $\mathbf{P_{s_{1/2}}}$ at the cell interface used in this work are discussed in [4].

4.5 Implicit time stepping

The resulting set of equations is a very stiff system since it has characteristic speeds ranging from the speed of sound of the different fluids to the speed of light. In order to deal with the strong time step requirements, implicit time stepping is applied. The second-order accurate three-point Backward Euler is used:

$$\frac{3}{2}\mathbf{U}^{n+1} - 2\mathbf{U}^n + \frac{1}{2}\mathbf{U}^{n-1} = \Delta t\ \mathbf{R}^{n+1} \tag{26}$$

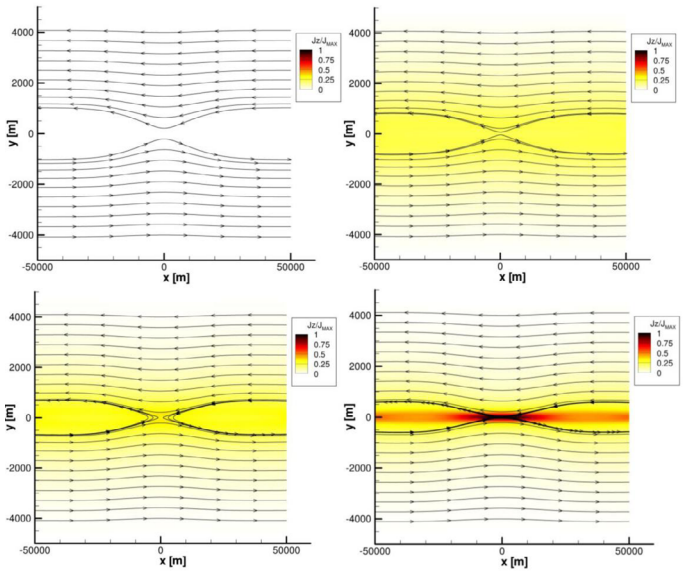

Figure 1: Evolution of the current sheet in the first seconds of simulation. Evolution of magnetic field lines and z-component of the electric current non-dimensionalized with its maximum value $J_{z_{MAX}} = 0.9475$ A/m^2. Top: from left to right, $t = 0$ s and $t = 5$ s. Bottom: from left to right, $t = 10$ s and $t = 20$ s.

5 RESULTS

The above mentioned model and numerical method are applied to investigate a reconnection scenario under chromospheric conditions. The computational domain extends from -5×10^4 m to 5×10^4 m in the x direction and -5×10^3 m to 5×10^3 m in the y direction. Periodic boundary conditions are used in the x-direction and perfectly conducting boundaries in the y-direction. The simulation domain is divided into 182000 cells (1400×130). The mesh stretches in the center, where the reconnection takes place, up to sizes of the order of one meter, comparable to the neutral-ion collision mean free path.

The initial conditions are chosen to be similar to chromospheric conditions estimated in the 1D model of the Sun [26]. The initial ion number density is $n_0 = 3.3 \times 10^{16} m^{-3}$ and the initial ionization level $n_i/(n_i + n_n) = 0.5\%$. The magnitude of the initial magnetic field is set to $10^{-3}T$ with oppositely directed fields in the x-component as follows: $B_x = -1{\times}10^{-3} \tanh(y/5000)$ T. The Spitzer resistivity is $\eta = 3.82{\times}10^{-3}\ \Omega m$.The temperature is set at 8750 K with a profile imposed to create a pressure that balances the initial Lorentz force $T_i'(y) = 4366.49/\cosh^2(y/5000)$ K and $T_n'(y) = 5443.43/\cosh^2(y/5000)$ K. All the components of the velocity are set to zero. This creates a balanced initial condition that is perturbed with a small ions velocity in the vertical direction: $v_i(y) = 20.1 \tanh(y/5000)/\cosh^2(y/5000)$ m/s and a small perturbation in the magnetic field around the center to initiate a reconnection at the center of the domain:

$B'_x = 8 \times 10^{-9} y e^{-(x/20000)^2-(y/5000)^2}$ T and $B'_y = -5 \times 10^{-10} x e^{-(x/20000)^2-(y/5000)^2}$ T.

In figure 1, the evolution of the current sheet and the magnetic field lines are shown. As can be seen, the magnetic lines change topology forming a current sheet in the center of the domain. The current width, δ , is defined to be the half-width at half-max of the current sheet. It is measured to be $\delta = 161$ m at $t = 20$ s. This value is of the same order of magnitude of the neutral-ion collision mean free path at this conditions $L_{ni} = v_{T,n}/\nu_{n,i} = 140$ m [1]. For all intensive purposes, the magnetic field has reconnected.

In figure 2, we compare the horizontal velocity of ions and neutrals. Since the geometry is symmetric, the ions are shown on the right and the neutrals on the left without loosing information. The neutrals are unaffected by the electromagnetic fields, however, the ions, that are accelerated by the Lorentz force driven by the current sheet, drag the neutrals through collisions. As can be seen, the horizontal velocity of ions and neutrals is very similar.

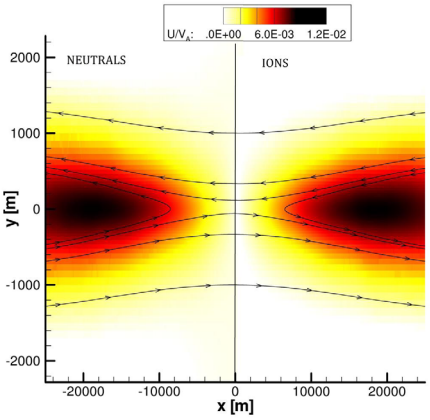

Figure 2: Horizontal velocity of neutrals and ions at $t = 20$ s. Non-dimensionalized with the value of the local Alfven speed outside the current sheet

.

However, in figure 3, we show that the vertical velocities and the streamtraces of ions and neutrals are clearly different. The maximum vertical velocity of the neutrals is shown to be 38.5% of the vertical velocity of the ions. This difference has a direct impact on the streamtraces, as shown in the bottom part of figure 3.

In figure 4 the densities of ions and neutrals are shown. The density of the ions change drastically from the initial field due to chemical reactions and also due to the compression produced by the electromagnetic forces.

6 CONCLUSIONS

The goal of the present research is to develop the numerical tools required to simulate the magnetic reconnection process with models that are able to overcome the limitations

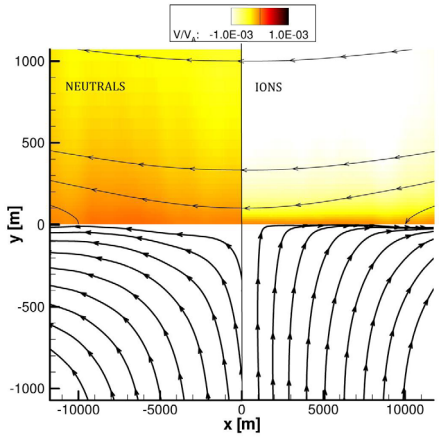

Figure 3: Vertical velocity and streamtraces of neutrals and ions at $t = 20$ s.

.

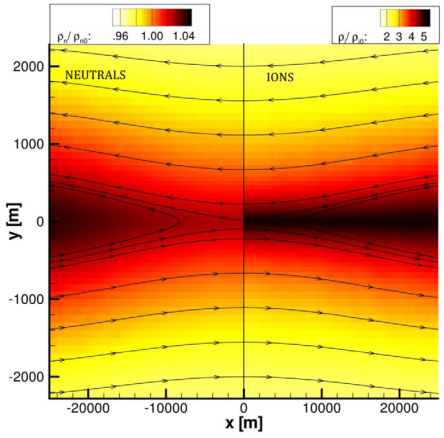

Figure 4: Density of neutrals and ions at $t = 20$ s. The values are non-dimensionalized with the initial values.

.

associated to standard single-fluid MHD models. Numerical algorithms for solving a multi-fluid model, considering charged particles and neutrals, coupled with full set of Maxwell equations have been presented in this work.

The FV method is applied to simulate a magnetic reconnection scenario with chromospheric conditions. Full set of Maxwell equations is considered, without neglecting the variation of the electric field in time that introduces electromagnetic fields. Hyperbolic divergence cleaning method is used to enforce the solenoidal constrains. For the fluids, AUSM$^+$-up method is implemented. In order to allow larger time steps, implicit second order time stepping is applied.

The results presented herein show how the magnetic field lines reconnect and a current sheet is created as a consequence of a small perturbation on an initial oppositely directed magnetic field with finite electrical resistivity of the charged fluid. We find that the electromagnetic forces accelerate the ions that drag the neutrals. The simulations show separation between the ions and neutrals vertical velocity due to the fact that the current sheet width is comparable to the neutral-ion collision mean free path. They also show how the densities of ions and neutrals evolve differently as a consequence of the chemical reactions and the electromagnetic forces.

REFERENCES

[1] J. E. Leake, V. Lukin, M. Linton, E. Meier, Multi-fluid simulations of chromospheric magnetic reconnection in a weakly ionized reacting plasma, *The Astrophysical Journal*, Volume 760, Issue 2, article id. 109, 2012.

[2] E. T. Meier, U. Shumlak, A general nonlinear fluid model for reacting plasma-neutral mixtures *Physics of Plasmas*, Volume 19, Issue 7, pp. 072508-072508-11, 2012.

[3] C. D. Munz, P. Ommes, R. Schneider, A three-dimensional finite-volume solver for the Maxwell equations with divergence cleaning on unstructured meshes, *Computer Physics Communications*, 130, 83-117, 1999.

[4] M. S. Liou, A sequel AUSM, part II: AUSM$^+$-up for all speeds. *Journal of Computational Physics*, 214:137-170, 2006.

[5] A. Lani, T. Quintino, D. Kimpe, H. Deconinck, S. Vandewalle, and S. Poedts, The COOLFluiD Framework: Design Solutions for High-Performance Object Oriented Scientific Computing Software, *Computational Science ICCS 2005*, edited by P. M. A. S. V. S. Sunderan, G. D. van Albada and J. J. Dongarra, Vol. **1** of *LNCS 3514*, Emory University, Springer, Atlanta, GA, USA, May 2005, pp. 281–286.

[6] A. Lani, T. Quintino, D. Kimpe, H. Deconinck, S. Vandewalle, and S. Poedts, Reusable Object-Oriented Solutions for Numerical Simulation of PDEs in a High Performance Environment, *Scientific Programming. Special Edition on POOSC 2005*, Vol. 14, No. 2, 2006, pp. 111–139.

[7] A. Lani, N. Villedieu, K. Bensassi, L. Kapa, M. Vymazal, M. S. Yalim and M. Panesi, COOLFluiD: an open computational platform for multi-physics simulation and research, 21th AIAA CFD Conference, San Diego (CA), Jun 2013.

[8] K. Shibata et al., *Chromospheric Anemone Jets as Evidence of Ubiquitous Reconnection*, Science, Volume 318, Issue 5856, pp. 1591, 2008.

[9] R. W. MacCormack *Numerical Simulation of Aerodynamic Flow Including Induced Magnetic and Electric Fields* 39th AIAA Plasmadynamics and Lasers Conference, Seattle, WA, AIAA Paper 2008-4010, 23-26 June 2008

[10] J. Birn and E. Priest, *Reconnection of Magnetic Fields*, Cambridge University Press, 2007.

[11] F. Zuccarello, *Data analysis and mathematical modeling of the initiation of coronal mass ejections*, PhD thesis, KU Leuven, 2012.

[12] M. Yamada, R. Kulsrud, and H. Ji, Magnetic Reconnection, *Reviews of Modern Physics* 82, 603, 2010.

[13] K. Shibata and T. Magara, *Solar Flares: Magnetohydrodynamic Processes*, Living Rev. Solar Phys. 8, 2011.

[14] E. N. Parker, *Sweet's mechanism for merging magnetic fields in conducting fluids*, Geophysical research 62, No. 4, 509-520, 1957

[15] H. E. Petschek. *Magnetic Annihilation*. The Physics of Solar Flares, Proceedings of the AAS-NASA Symposium, October 1963

[16] D. Biskamp, *Magnetic Reconnection in Plasmas*, Cambridge University Press, 2005

[17] S. I. Braginskii, *Transport processes in a plasma*. Reviews of Plasma Physics, Volume 1., pp. 205 311. (1965)

[18] B. Graille , T. E. Magin , M. Massot, *Kinetic theory of plasmas. Translational Energy.* Mathematical Models and Methods in Applied Sciences, Vol. 19, 04 (2009) 527-599

[19] A. Lani, *An object Oriented and high performmance platform for aerothermodynamics simulations*, PhD Thesis, von Karman Institute for Fluid Dynamics, 2009

[20] T. Barth. *Aspects of unstructured grids and finite volume solvers for the euler and navier-stokes equations.* 25th Computational Fluid Dynamics Lecture Series. Von Karman Institute, March 1994.

[21] V. Venkatakrishnan. *Convergence to steady state solutions of the euler equations on unstructured grids with limiters.* Journal of Computational Physics, 118:120130, 1995.

[22] J. Steger, R. F. Warming, *Flux vector splitting for the inviscid gas dynamic equations with application to finite difference methods*, J. Comp. Phys., Vol. 40, No. 2, pp. 263-293, 1981

[23] A. Alvarez, *Multi-Fluid MHD Development for Space Weather Modeling*, Research Master Report, von Karman Institute for Fluid Dynamics, June 2013.

[24] G. S. Voronov, *A practical fit formula for ionization rate coefficients of atoms and ions by electron impact*, Atomic data and nuclear data tables 65, 1-35, 1997

[25] B. M. Smirnov, *Physics of Atoms and Ions*, Springer-Verlag New York, Inc., 2003

[26] Vernazza, J. E., Avrett, E. H., Loeser, R., *Structure of the solar chromosphere. III. Models of the EUV brightness components of the quiet Sun*, ApJS45, 635-725, 1981